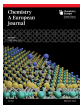

Covalent Patterning of 2D MoS_2

Xin Chen,[a] Malte Kohring,[b] M'hamed Assebban,[a] Bartłomiej Tywoniuk,[c] Cian Bartlam,[c] Narine Moses Badlyan,[b] Janina Maultzsch,[b] Georg S. Duesberg,[c] Heiko B. Weber,[b] Kathrin C. Knirsch,[a] and Andreas Hirsch*[a]

Abstract: The development of an efficient method to patterning 2D MoS_2 into a desired topographic structure is of particular importance to bridge the way towards the ultimate device. Herein, we demonstrate a patterning strategy by combining the electron beam lithography with the surface covalent functionalization. This strategy allows us to generate delicate MoS_2 ribbon patterns with a minimum feature size of 2 μm in a high throughput rate. The patterned monolayer MoS_2 domain consists of a spatially well-defined heterophase homojunction and alternately distributed surface characteristics, which holds great interest for further exploration of MoS_2 based devices.

Two-dimensional (2D) transition metal dichalcogenides (TMDCs) are deemed promising for the next generation semiconductor platforms owing to their extraordinary properties.[1–2] As a representative, monolayer MoS_2 - a direct bandgap semiconductor - is one of the most appealing 2D TMDCs due to its exceptional physical properties and potential applications in electronic and optoelectronic devices.[3–6] Patterning of the 2D MoS_2 surface is a crucial step towards further integration of MoS_2 into miniaturized devices.[7] Patterned MoS_2 nanostructures have been obtained through either bottom-up or top-down strategies. The bottom-up strategies usually involve the growth or self-assembly of molecular building blocks onto the pre-defined substrates;[8–10] the top-down strategies use lithographic techniques to engineer the morphology, phase, shape and chemical composition of the material surface towards the desired geometry and device properties.[11–19] Combining the bottom-up surface chemistry with the top-down lithographic technologies allows controlling the patterned structures in a more versatile and precise manner, facilitating efficient manufacture. So far, such a concept has applied in graphene systems,[20–21] yet rarely to a 2D MoS_2 surface.[22]

The functionalization chemistry of the inert MoS_2 basal plane has been a burgeoning field in recent years. A variety of inorganic and organic compounds is employed to modify the MoS_2 surface.[23–24] Yet, only a few types of reagents such as diazonium salts,[25] organohalides,[26] and maleimides[27] can form robust covalent bonds with the MoS_2 surface. Among them, diazonium salts are the most extensively used ones. The high reactivity of diazonium salts enables the coupling of functional groups on both pristine[28] and activated MoS_2 surface.[25,29–30] The reactions between activated MoS_2 and diazonium salts can lead to a high degree of functionalization in a short reaction time. For example, the maximum degree of functionalization can reach 40% per sulfur atom.[30] Moreover, the properties of the functionalized surface can be systematically tuned by varying the functional groups.[30] These advantages of the diazonium chemistry based surface modification, and its compatibility with other lithographic techniques, have made it ideal for covalent patterning of the MoS_2 surface.

Herein, we demonstrate an efficient approach to patterning 2D MoS_2 through covalent functionalization of electron beam lithography (EBL) defined guiding patterns. This approach leads to the formation of high-quality, patterned MoS_2 ribbons with a minimum feature size of 2 μm in a high throughput rate. The covalent functionalization reaction introduced here allows modifying the phase and chemical composition of MoS_2 in one development process. The resulting patterned MoS_2 displays switchable surface characteristics and a lateral heterophase in a spatially defined manner, confirmed by scanning Raman spectroscopy and photoluminescence (PL) mapping.

The principle of covalent functionalization of 2D MoS_2 on Si/SiO_2

Figure 1a describes the main steps of covalent functionalization of MoS_2 on Si/SiO_2. The MoS_2 deposited on Si/SiO_2 was initially activated, resulting in the negatively charged MoS_2. Then the activated MoS_2 was reacted with the electrophile, 4-bromobenzenediazonium tetrafluoroborate, yielding the functionalized

[a] Dr. X. Chen, Dr. M'h. Assebban, Dr. K. C. Knirsch, Prof. A. Hirsch
Department of Chemistry and Pharmacy
Friedrich-Alexander-Universität Erlangen-Nürnberg (FAU)
Nikolaus-Fiebiger-Straße 10, 91058 Erlangen (Germany)
E-mail: andreas.hirsch@fau.de

[b] M. Kohring, N. Moses Badlyan, Prof. J. Maultzsch, Prof. H. B. Weber
Department of Physics
Friedrich-Alexander-Universität Erlangen-Nürnberg (FAU)
Staudtstr.7, 91058 Erlangen (Germany)

[c] Dr. B. Tywoniuk, Dr. C. Bartlam, Prof. G. S. Duesberg
Institute of Physics, EIT 2
Faculty of Electrical Engineering and Information Technology
Universität der Bundeswehr
85579 Neubiberg (Germany)

Supporting information for this article is available on the WWW under https://doi.org/10.1002/chem.202102021

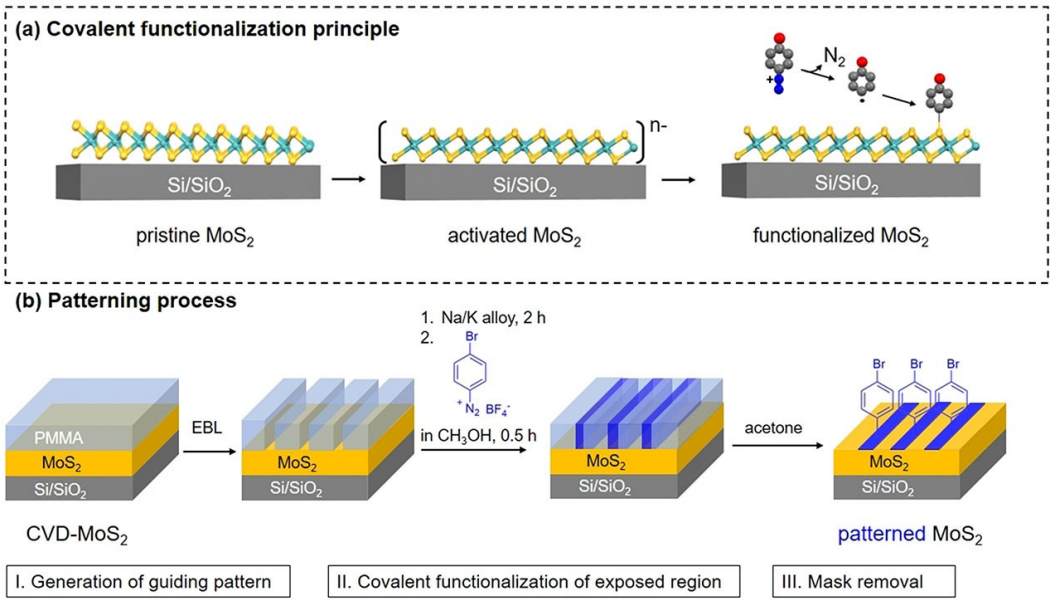

Figure 1. Covalent patterning of MoS_2 surface. (a) The concept for covalent functionalization of 2D MoS_2 on Si/SiO_2 via a reductive pathway. (b) Schematic illustration of the patterning process on CVD-MoS_2 surface: I. Generation of guiding pattern by selective removal of the PMMA mask at designed locations using electron beam lithography (EBL); II. The unmasked region was then activated using Na/K alloy followed by the functionalization reaction with 4-bromobenzenediazonium salts whereas the masked region was preserved; III. Removal of PMMA mask in acetone bath, resulting in the pristine and functionalized MoS_2 ribbons alternately distributed on the patterned domain.

MoS_2. To evaluate the feasibility of this concept, we first performed a proof-of-concept study using mechanically exfoliated MoS_2 (me-MoS_2) samples (Figure S1a). Activating MoS_2 on Si/SiO_2 (100 nm) was achieved by covering the surface of MoS_2 with Na/K alloy under argon atmosphere for 2 h. The wettability and the solvent-free nature of Na/K alloy reductant ensure the efficient reduction of MoS_2[24] and easy purification. The follow-up reaction of activated MoS_2 with 4-bromobenzenediazonium tetrafluoroborate was completed by immersion of the activated film into a 4-bromobenzenediazonium tetrafluoroborate/ anhydrous methanol solution under argon atmosphere (see Supporting Information for details). The optical images (Figure S1b) show a color change of MoS_2 flakes from green to blue, indicating a change of optical properties upon functionalization. Elemental mapping of functionalized MoS_2 (B-MoS_2, where B denotes the 4-bromophenyl group) nanosheets (Figure S2) using scanning electron microscopy coupled energy dispersive X-ray spectroscopy (SEM-EDS) shows evenly distributed carbon and bromine signals over the flakes, verifying the successful incorporation of bromophenyl functional groups to the MoS_2 surface.

Comparison of the Raman spectra ($\lambda_{exc} = 633$ nm) of B-MoS_2 to pristine me-MoS_2 (Figure S4a) reveals two additional peaks at 150 and 226 cm^{-1} in B-MoS_2, corresponding to the J_1 and J_2 modes of 1T-phase MoS_2. This demonstrates that 1T-phase was present in B-MoS_2, which was consistent with other reductive functionalization studies.[25–26,29] Noticeably, the peak at 226 cm^{-1} can also be assigned to LA mode associated with the defects of the MoS_2 lattice.[31–32] Previous studies have pointed out that the intensity of this peak relative to either the E^1_{2g} or A_{1g} mode of MoS_2 linearly correlates to the density of defects, similar to the D/G intensity ratio in the graphene system.[31] Our recent experimental study also verified that the activation of this phonon mode was indeed related to the surface functionalization.[33]

Bearing this in mind, we used the relative intensity of the LA mode as a probe to identify the ideal reaction conditions for covalent functionalization. We performed a control experiment by reacting me-MoS_2 directly with diazonium salts without activation (Figure S3). The Raman spectrum of a functionalized sample prepared without activation (Figure S3d, black trace) displays a much lower intensity of the LA mode compared to that prepared with activation (Figure S3d, red trace). In particular, for the functionalized MoS_2 prepared with activation (B-MoS_2), the intensity of the LA mode relative to E^1_{2g} mode was more than three times higher than that for the sample prepared without activation (b-MoS_2, see detailed data in Table S1). As a higher relative intensity of the LA mode reflects a higher density of defects (surface addends), the control experiment demonstrates that activation of MoS_2 film before functionalization is the key to obtain efficient functionalization. Achieving a high degree of functionalization on the defined surface area is necessary because it will enable a better contrast to the pristine surface area, which favors a well-resolved pattern in the following study.

In addition, we monitored the Raman spectrum of B-MoS_2 at extended reaction time (Figure S4a) and plotted the peak intensity ratios of LA/E^1_{2g} and LA/A_{1g} as a function of the reaction time (Figure S4b). Interestingly, the relative intensity of the LA mode increased by eight fold compared to the pristine

me-MoS_2 when the reaction underwent 30 min. However, extending the reaction time did not increase the relative peak intensity of the LA mode further, implying that the degree of functionalization was saturated after 30 min.

Covalent patterning of a CVD-grown MoS_2 surface

A schematic illustration of the patterning process on the chemical vapor deposition (CVD) grown MoS_2 surface is depicted in Figure 1b. The CVD-MoS_2 on Si/SiO_2 (300 nm) was firstly spin-coated with a layer of electron beam resist mask, poly (methyl methacrylate) (PMMA). Then the guiding pattern (Figure 2a) was created by selective removal of the PMMA mask at designed locations using electron beam lithography (EBL). The subsequent activation with Na/K alloy followed by the reaction with 4-bromobenzenediazonium salts allowed the unmasked areas to be functionalized, whereas the masked areas were preserved. The resulting film was thoroughly washed with methanol and water to remove all the physiosorbed residues. After removal of PMMA mask by acetone, the patterned MoS_2 surface was characterized by optical microscopy, atomic force microscopy (AFM), SEM-EDS, Raman spectroscopy, and photoluminescence (PL) spectroscopy (see Supporting Information for details).

The AFM image of the patterned MoS_2 surface after removal of PMMA (Figure 2b) shows a preserved structure in the functionalized region but a damaged structure in the pristine MoS_2 region, suggesting the surface modification improved the robustness of the MoS_2 surface against the possible delamination or fracture during the purification steps. Taking the surface roughness into consideration, a clear variation of height (inset height profile, Figure 2b) between the functionalized MoS_2 stripes (pointed out by the blue arrows) and pristine MoS_2 gap can still be identified along the measured region. In particular, two functionalized stripes maintain roughly the same height, about 1.2 nm thicker than the pristine MoS_2 gap. A height increase of functionalized MoS_2 stripes relative to the pristine MoS_2 gap was possibly due to the joint effect of intercalation and surface covalent functionalization.[28,34] We further characterized the patterned MoS_2 surface under ambient conditions by Kelvin probe force microscopy (KPFM). The surface potential map (Figure S5a) displays an alternately distributed ribbon pattern, suggesting a clear surface potential variation between the functionalized and pristine MoS_2 regions. The dramatic variation of surface potential (Figure S5b) can be attributed to significant change of electronic properties caused by the intercalation and chemical functionalization.[35–37]

The SEM image of the patterned MoS_2 surface (Figure 3a and b) displays clear boundaries between functionalized and pristine MoS_2 regions. Elemental mapping of the patterned MoS_2 surface using EDS shows discernible C and Br signals (Figure 3c), originated from the introduced bromophenyl functional groups. In particular, the C and Br signals accumulated in the unmasked region of the guiding pattern (Figure 3d and Figure S6), suggesting that the functional groups were only bounded to the unmasked MoS_2 surface. The moderate signal to noise ratio in Figure S6b was likely related to the lower content of Br (1/6 of C).

Raman spectra of both pristine CVD-MoS_2 (Figure 4a, black trace) and functionalized MoS_2 ribbons (Figure 4a, red trace) show the characteristic E^1_{2g}, A_{1g}, and 2LA modes. Unlike pristine CVD-MoS_2, the functionalized MoS_2 ribbons show additional phonon modes at 153, 226 and 352 cm^{-1}, corresponding to the J_1, J_2, and J_3 modes of 1T-phase, demonstrating the presence of a 1T-phase in the functionalized MoS_2 ribbons. Interestingly, compared to the pristine CVD-MoS_2, the Raman spectrum of functionalized MoS_2 ribbons shows significantly increased intensity of the LA mode, suggesting a high degree of functionalization. The Raman line mapping of the intensity ratio of LA to E^1_{2g} (or A_{1g}) (Figure S7a and S7b) vividly resembles the location and the width of the functionalized MoS_2 ribbons, which correlates well with the optical image of the patterned MoS_2 surface (Figure S7c). In specific, the functionalized ribbons corresponding to the regions with high intensity ratios can be easily identified.

Importantly, by applying our covalent patterning approach, a large area ($100 \times 100\ \mu m^2$) and high quality of MoS_2 surface

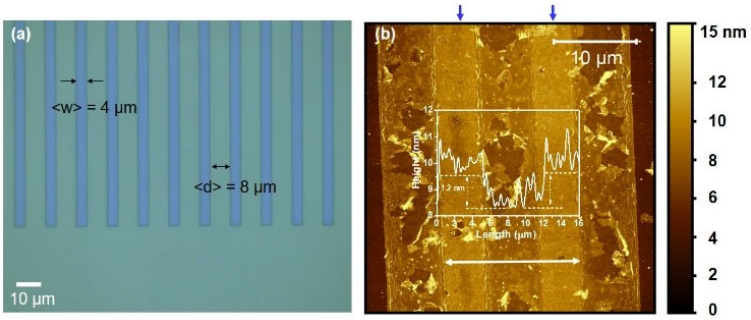

Figure 2. (a) Optical image of CVD-MoS_2 coated with PMMA after EBL patterning. The width of each unmasked MoS_2 ribbon is 4 µm. The width of the masked interspace is 8 µm. (b) AFM image of patterned MoS_2 surface after removal of PMMA. While the structure of functionalized MoS_2 ribbons (marked with blue arrows) remains mostly intact, the pristine MoS_2 surface shows fracture after the purification steps. The inset height profile of the measured region (marked with white arrow) indicates that the thickness of functionalized MoS_2 ribbons increased by 1.2 nm compared to pristine MoS_2.

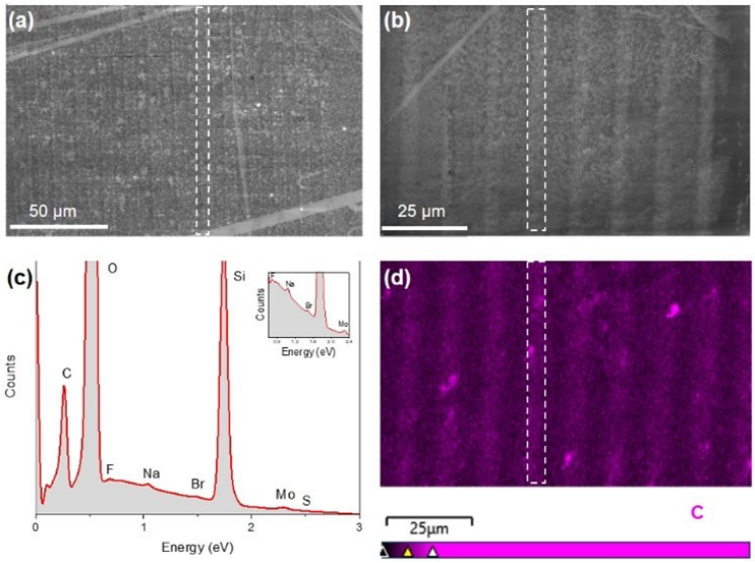

Figure 3. SEM-EDS characterization of patterned CVD-MoS_2 surface after removal of PMMA. (a–b) SEM images of patterned CVD-MoS_2 surface under the varied magnification. (c) Elemental composition of patterned CVD-MoS_2 surface. The inset shows the presence of Br in the detected region. (d) EDS mapping image of C distribution. The dashed block in (a, b, and d) indicates one of the functionalized MoS_2 ribbons.

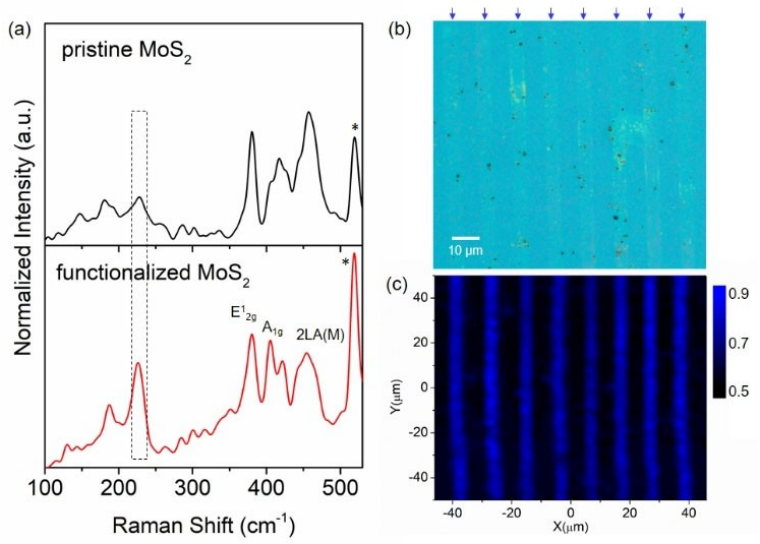

Figure 4. (a) Raman spectra ($\lambda = 633$ nm) of pristine (black) and functionalized (red) regions on the CVD-MoS_2 surface. The spectra were subjected to the baseline subtraction and normalized to the intensity of E^1_{2g} mode for comparison. The peaks marked with an asterisk are Raman modes of the underlying Si/SiO_2 substrate. The dashed block highlights the functionalization related LA mode at 226 cm^{-1}. (b) Optical image of the patterned CVD-MoS_2 surface after removal of PMMA: the functionalized MoS_2 ribbons (light green, marked with blue arrows) and pristine MoS_2 gaps (cyan) are alternately distributed. (c) Raman spatial map of the intensity ratio (LA/E^1_{2g}) on the patterned CVD-MoS_2 surface. The functionalized MoS_2 ribbons with high intensity ratios are shown as blue stripes.

with a delicate pattern can be generated (Figure 4b). The Raman spatial mapping of the intensity ratio of LA to E^1_{2g} displays a well-resolved pattern (Figure 4c), wherein the functionalized ribbons with high intensity ratios and the pristine MoS_2 gaps with low intensity ratios are alternately distributed. The Raman map with the gradient color scale (Figure S7d) displays higher relative intensity of LA mode in the center of the functionalized ribbons compared to the edges, suggesting that the center of the functionalized surface shows a higher degree of functionalization. One possible reason for the variation of the degree of functionalization could be: the center of the exposed MoS_2 surface, rich in defects (Figure 2b), triggers the initial binding of functional groups onto MoS_2. The tethered addends then act as nucleation centers, facilitating the proliferation of the addends over the surface. The mechanism about the propagation of functionalization along the defects has been monitored and investigated in details by another group.[28]

Having the covalently patterned MoS_2 surface in hand, we then examined the PL behavior of this structured construct. The PL spectrum of pristine CVD-MoS_2 (Figure 5a) displays one predominant peak at 1.88 eV and a small shoulder at 2.02 eV, attributed to the A exciton and B exciton, respectively. In comparison, the functionalized MoS_2 ribbons show a significantly decreased intensity with a slightly down-shifted peak position of the A exciton, which was likely due to the collective effect of phase transformation (2H-phase to 1T-phase)[26,38] and *n*-doping. The *n*-doping induced PL evolution has been reported in other functionalized MoS_2 systems as well.[28,39–40] Similar phenomena can also be observed when comparing the PL spectra of the same CVD-MoS_2 sample before and after electron beam bombardment (Figure S8).

Besides, the contribution of the B exciton became more pronounced in the functionalized MoS_2 region than in the pristine MoS_2 region, which was likely attributed to the presence of higher density of non-radiative defects (functionalized surface)[41] in the functionalized MoS_2 region. The functionalized MoS_2 ribbons can be distinguished as the high intensity bright stripes in the PL intensity map of B exciton (Figure 5c) and the low intensity dark stripes in the PL intensity map of A exciton (Figure 5b). The switchable PL response of patterned MoS_2 surface signifies the potential to specially modulate the optical properties of MoS_2 via covalent functionalization. By applying this covalent patterning approach, we can pattern more complicated structures. For example, the FAU logo was created through EBL followed by covalent patterning process (Figure S9). This pattern featured with the minimum width of a character of 2 μm can be visualized through PL intensity mapping of the A and B exciton.

In summary, we demonstrated an effective method for covalent patterning of MoS_2 surface. By combining EBL with diazonium chemistry directed surface functionalization, we generated high-quality and well-defined patterns with a minimum feature size of 2 μm on the CVD grown MoS_2 surface. The resulting patterned MoS_2 surface displays switchable surface characteristics in a spatially defined manner, confirmed by scanning Raman spectroscopy and PL mapping, which may hold great promise for the development of state-of-the-art electronic and optoelectronic devices. The covalent patterning method opens a convenient avenue for spatially designing, engineering, and derivatizing MoS_2 nanostructures, which would benefit further exploration of surface chemistry of MoS_2-like 2D platforms and facilitate efficient manufacture.

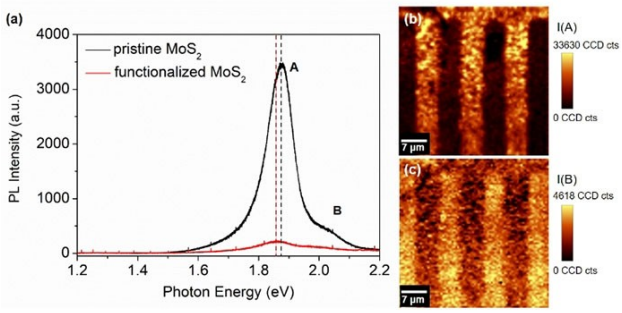

Figure 5. (a) PL spectra (λ = 532 nm) of pristine and functionalized MoS_2 regions on the patterned CVD-MoS_2 surface. The dashed lines indicate the peak position of the A exciton in pristine (black) and functionalized (red) MoS_2. (b) PL intensity map of the A exciton. (c) PL intensity map of the B exciton.

Acknowledgements

This project has received funding from the European Union's Horizon 2020 research and innovation programme Graphene Flagship under grant agreement No 881603 and the Deutsche Forschungsgemeinschaft (DFG, German Research Foundation), Projektnummer 182849149-SFB 953 "Synthetic Carbon Allotropes"- A1, B8, and B13. G. S. Duesberg, B. Tywoniuk, and C. Bartlam thank the EU H2020 under contract No. 829035 (QUEFORMAL) for support. Open access funding enabled and organized by Projekt DEAL.

Conflict of Interest

The authors declare no conflict of interest.

Keywords: functionalization · MoS_2 · patterning · PL · Raman spectroscopy

[1] B. Radisavljevic, A. Radenovic, J. Brivio, V. Giacometti, A. Kis, *Nat. Nanotechnol.* **2011**, *6*, 147–150.
[2] M. Chhowalla, H. S. Shin, G. Eda, L. J. Li, K. P. Loh, H. Zhang, *Nat. Chem.* **2013**, *5*, 263–275.
[3] K. F. Mak, K. He, C. Lee, G. H. Lee, J. Hone, T. F. Heinz, J. Shan, *Nat. Mater.* **2013**, *12*, 207–211.
[4] H. Yang, S. W. Kim, M. Chhowalla, Y. H. Lee, *Nat. Phys.* **2017**, *13*, 931–937.
[5] D.-H. Lien, S. Z. Uddin, M. Yeh, M. Amani, H. Kim, J. W. Ager, E. Yablonovitch, A. Javey, *Science* **2019**, *364*, 468–471.
[6] G. M. Marega, Y. Zhao, A. Avsar, Z. Wang, M. Tripathi, A. Radenovic, A. Kis, *Nature* **2020**, *587*, 72–77.
[7] M. G. Stanford, P. D. Rack, D. Jariwala, *NPJ 2D Mater. Appl.* **2018**, *2*, 20.
[8] Y. Guo, P.-C. Shen, C. Su, A.-Y. Lu, M. Hempel, Y. Han, Q. Ji, Y. Lin, E. Shi, E. McVay, L. Dou, D. A. Muller, T. Palacios, J. Li, X. Ling, J. Kong, *Proc. Nat. Acad. Sci.* **2019**, *116*, 3437–3442.
[9] M. S. M. Saifullah, M. Asbahi, M. Binti-Kamran Kiyani, S. S. Liow, S. Bin Dolmanan, A. M. Yong, E. A. H. Ong, A. Ibn Saifullah, H. R. Tan, N. Dwivedi, T. Dutta, R. Ganesan, S. Valiyaveettil, K. S. L. Chong, S. Tripathy, *ACS Appl. Mater. Interfaces* **2020**, *12*, 16772–16781.
[10] C. Martella, L. Ortolani, E. Cianci, A. Lamperti, V. Morandi, A. Molle, *Nano Res.* **2019**, *12*, 1851–1854.
[11] J. Zhao, H. Yu, W. Chen, R. Yang, J. Zhu, M. Liao, D. Shi, G. Zhang, *ACS Appl. Mater. Interfaces* **2016**, *8*, 16546–16550.
[12] A. Nourbakhsh, A. Zubair, R. N. Sajjad, A. Tavakkoli, K. G. W. Chen, S. Fang, X. Ling, J. Kong, M. S. Dresselhaus, E. Kaxiras, K. K. Berggren, D. Antoniadis, T. Palacios, *Nano Lett.* **2016**, *16*, 7798–7806.
[13] M. G. Stanford, Y.-C. Lin, M. G. Sales, A. N. Hoffman, C. T. Nelson, K. Xiao, S. McDonnell, P. D. Rack, *NPJ 2D Mater. Appl.* **2019**, *3*, 13.
[14] J. Zhu, Z. Wang, H. Yu, N. Li, J. Zhang, J. Meng, M. Liao, J. Zhao, X. Lu, L. Du, R. Yang, D. Shi, Y. Jiang, G. Zhang, *J. Am. Chem. Soc.* **2017**, *139*, 10216–10219.
[15] H. Zhang, B. Abhiraman, Q. Zhang, J. Miao, K. Jo, S. Roccasecca, M. W. Knight, A. R. Davoyan, D. Jariwala, *Nat. Commun.* **2020**, *11*, 3552.
[16] P. S. Kollipara, J. Li, Y. Zheng, *Research* **2020**, *2020*, 6581250.
[17] J. Lin, O. Cretu, W. Zhou, K. Suenaga, D. Prasai, K. I. Bolotin, N. T. Cuong, M. Otani, S. Okada, A. R. Lupini, J.-C. Idrobo, D. Caudel, A. Burger, N. J.

Ghimire, J. Yan, D. G. Mandrus, S. J. Pennycook, S. T. Pantelides, *Nat. Nanotechnol.* **2014**, *9*, 436–442.
[18] G. Yao, D. Zhao, Y. Hong, S. Wu, D. Liu, M. Qiu, *Nanoscale* **2020**, *12*, 22473–22477.
[19] D. S. Fox, Y. Zhou, P. Maguire, A. O'Neill, C. Ó'Coileáin, R. Gatensby, A. M. Glushenkov, T. Tao, G. S. Duesberg, I. V. Shvets, M. Abid, M. Abid, H.-C. Wu, Y. Chen, J. N. Coleman, J. F. Donegan, H. Zhang, *Nano Lett.* **2015**, *15*, 5307–5313.
[20] F. M. Koehler, N. A. Luechinger, D. Ziegler, E. K. Athanassiou, R. N. Grass, A. Rossi, C. Hierold, A. Stemmer, W. J. Stark, *Angew. Chem. Int. Ed.* **2009**, *48*, 224–227; *Angew. Chem.* **2008**, *121*, 230–233.
[21] L. Bao, M. Kohring, H. B. Weber, F. Hauke, A. Hirsch, *J. Am. Chem. Soc.* **2020**, *142*, 16016–16022.
[22] P. Zhao, R. Wang, D.-H. Lien, Y. Zhao, H. Kim, J. Cho, G. H. Ahn, A. Javey, *Adv. Mater.* **2019**, *31*, 1900136.
[23] X. Chen, A. R. McDonald, *Adv. Mater.* **2016**, *28*, 5738–5746.
[24] S. Bertolazzi, M. Gobbi, Y. Zhao, C. Backes, P. Samorì, *Chem. Soc. Rev.* **2018**, *47*, 6845–6888.
[25] K. C. Knirsch, N. C. Berner, H. C. Nerl, C. S. Cucinotta, Z. Gholamvand, N. McEvoy, Z. Wang, I. Abramovic, P. Vecera, M. Halik, S. Sanvito, G. S. Duesberg, V. Nicolosi, F. Hauke, A. Hirsch, J. N. Coleman, C. Backes, *ACS Nano* **2015**, *9*, 6018–6030.
[26] D. Voiry, A. Goswami, R. Kappera, C. de Carvalho Castro e Silva, D. Kaplan, T. Fujita, M. Chen, T. Asefa, M. Chhowalla, *Nat. Chem.* **2015**, *7*, 45–49.
[27] M. Vera-Hidalgo, E. Giovanelli, C. Navío, E. M. Pérez, *J. Am. Chem. Soc.* **2019**, *141*, 3767–3771.
[28] X. S. Chu, A. Yousaf, D. O. Li, A. A. Tang, A. Debnath, D. Ma, A. A. Green, E. J. G. Santos, Q. H. Wang, *Chem. Mater.* **2018**, *30*, 2112–2128.
[29] E. Er, H. Hou, A. Criado, J. Langer, M. Möller, N. Erk, L. M. Liz-Marzán, M. Prato, *Chem. Mater.* **2019**, *31*, 5725–5734.
[30] E. E. Benson, H. Zhang, S. A. Schuman, S. U. Nanayakkara, N. D. Bronstein, S. Ferrere, J. L. Blackburn, E. M. Miller, *J. Am. Chem. Soc.* **2018**, *140*, 441–450.
[31] S. Mignuzzi, A. J. Pollard, N. Bonini, B. Brennan, I. S. Gilmore, M. A. Pimenta, D. Richards, D. Roy, *Phys. Rev. B* **2015**, *91*, 195411.
[32] Q. Qian, Z. Zhang, K. J. Chen, *Langmuir* **2018**, *34*, 2882–2889.
[33] X. Chen, C. Bartlam, V. Lloret, N. Moses Badlyan, S. Wolff, R. Gillen, T. Stimpel-Lindner, J. Maultzsch, G. S. Duesberg, K. C. Knirsch, A. Hirsch, *Angew. Chem. Int. Ed.* **2021**, *60*, 13484–13492.
[34] C. R. Ryder, J. D. Wood, S. A. Wells, Y. Yang, D. Jariwala, T. J. Marks, G. C. Schatz, M. C. Hersam, *Nat. Chem.* **2016**, *8*, 597–602.
[35] K. Jo, P. Kumar, J. Orr, S. B. Anantharaman, J. Miao, M. J. Motala, A. Bandyopadhyay, K. Kisslinger, C. Muratore, V. B. Shenoy, E. A. Stach, N. R. Glavin, D. Jariwala, *ACS Nano* **2021**, *15*, 5618–5630.
[36] D. Moore, K. Jo, C. Nguyen, J. Lou, C. Muratore, D. Jariwala, N. R. Glavin, *NPJ 2D Mater. Appl.* **2020**, *4*, 44.
[37] M. Z. Hossain, M. A. Walsh, M. C. Hersam, *J. Am. Chem. Soc.* **2010**, *132*, 15399–15403.
[38] G. Eda, H. Yamaguchi, D. Voiry, T. Fujita, M. Chen, M. Chhowalla, *Nano Lett.* **2011**, *11*, 5111–5116.
[39] H. Ichimiya, M. Takinoue, A. Fukui, T. Yoshimura, A. Ashida, N. Fuji-mura, D. Kiriya, *ACS Appl. Mater. Interfaces* **2019**, *11*, 15922–15926.
[40] Y. Wang, S. M. Gali, A. Slassi, D. Beljonne, P. Samorì, *Adv. Funct. Mater.* **2020**, *30*, 2002846.
[41] K. M. McCreary, A. T. Hanbicki, S. V. Sivaram, B. T. Jonker, *APL Mater.* **2018**, *6*, 111106.

Manuscript received: June 8, 2021
Version of record online: August 6, 2021

